Reconstruction for Proton Computed Tomography: A Monte Carlo Study

T Li, Z. Liang, K. Mueller, J. Heimann, L. Johnson,
H. Sadrozinski, A. Seiden, D. Williams, L. Zhang,
S. Peggs, T. Satogata, V. Bashkirov, and R. Schulte

***Abstract* --** Advantages of proton computed tomography (pCT) have been recognized in the past. However, the quality of a pCT image may be limited due to the stochastic nature of the proton path inside the object. In this work, we report a preliminary study on reconstruction of pCT image with improved path estimation. A set of Monte Carlo simulations was carried out with the GEANT4 program, and reconstructed by filtered backprojection method. Simulations with different density contrast settings were compared, and spatial resolution around 0.5mm for the highest contrast phantom was achieved, which is comparable to that of x-ray CT image. Further improvement by utilizing the statistical properties of proton transport is expected and is under progress.

I. Introduction

PROTON computed tomography (pCT) has two major possible advantages in medical applications. First for diagnosis, its low-dose advantage might be utilized effectively to provide CT image reconstruction with significantly better density contrast resolution than x-ray CT (xCT) at a given dose level. Its unique imaging characteristics based on linear stopping power of charged particles, as compared to the x-ray attenuation coefficient, may prove beneficial in medical diagnosis. Secondly, a successful implementation of pCT would avoid or simplify many of the current tedious procedures for proton therapy, including xCT imaging, mapping of xCT numbers to proton stopping power values, moving and repositioning the patient, and patient position-checking in the treatment room [1, 2].

A conceptual pCT system, which is similar to the first generation of xCT, is illustrated in Fig. 1. The data scanning is accomplished by translation and rotation operations. Instead of x-rays, pCT utilizes a high energy (100-250 MeV) proton beam that penetrates the object. It is important that the protons have sufficient energy to penetrate the thickest part of the object.

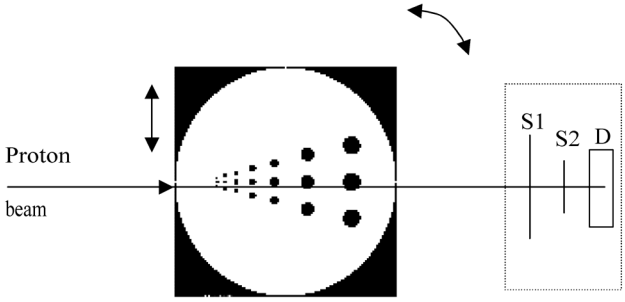

Fig. 1. Schematic diagram of a conceptual pCT system. The proton pencil beam and detectors remain stationary while the object moves and rotates. The detection part includes two position sensitive silicon detectors (S1 and S2), and a scintillation detector (D) to measure the residual proton energy.

One merit of proton imaging techniques is that the particles can be detected one-by-one, avoiding the quantum noise of xCT imaging. With present technologies, both the location and direction of each entrance and exit proton can be recorded as well as the energy of each exit proton, while the entrance energy is presumed to be known with excellent accuracy. This provides more information than xCT, and may be beneficial for image reconstruction.

In general, the reconstruction task of charge particles distinguishes itself from others by the stochastic path of the particles inside the body. Numerous small angle deflections

Manuscript received October 20, 2003. This work was supported in part by the NIH National Heart, Lung and Blood Institute under Grant No. HL54166, the Calspace and the National Medical Technology Testbed Inc (NMTB) under the U.S. Department of the Army Medical Research Acquisition Activity, the Cooperative Agreement DAMD17-972-7016, and the U.S. Department of Energy contract No: DE-AC02-98ch10886. The views and conclusions contained in this presentation are those of the authors and do not necessarily reflect the position or the policy of the U.S. Army or NMTB.

T. Li, Z. Liang, and K. Mueller are with the Departments of Physics and Astronomy, Radiology, and Computer Science, State University of New York, Stony Brook, NY 11790 USA. (631-444-7999, Email: tfli@mil.sunysb.edu).

J. Heimann, L. Johnson, H. Sadrozinski, A. Seiden, D. Williams, and L. Zhang are with the Santa Cruz Institute for Particle Physics, University of California, Santa Cruz, CA 95064 USA.

S. Peggs and T. Satogata are with the Collider-Accelerator Department, Brookhaven National Lab, Upton, NY 11973 USA.

V. Bashkirov and R. Schulte are with the Department of Radiation Medicine, Loma Linda University Medical Center, Loma Linda, CA 92354 USA.

by the Coulomb field of the nuclei make the estimation of the proton path very challenging. Therefore, the reconstruction of pCT from measurement of proton energy-loss encounters a resolution limit due to these deflections.

In this work, a set of Monte Carlo (MC) simulations was carried out for pCT using an aluminum phantom with multiple holes and different contrast settings. An ideal beam of parallel, monoenergetic protons was assumed. Given exact knowledge of the entry position of each proton and its exit position and direction, the path of the proton inside the body was approximated by a straight line. After a bilinear interpolation to satisfy the requirements of Radon transform, the reconstruction was performed very efficiently by the conventional filtered backprojection (FBP) method. The results show satisfactory image quality comparable to that of xCT imaging for this relatively ideal scenario. Further study on how to correct the energy loss based on the path divergence and its statistical distribution is in progress.

II. Background Theories

A. Principle of Proton CT

The main principle of pCT is based on the determination of the integrated volume electron density, ρ_e, by measuring the energy loss of protons after traversing the image object. The volume electron density of a medium is defined as the number of electrons/cm^3. The relationship between volume electron density and physical density is given by

$$\rho_e = \rho N_A \left(\frac{Z}{A}\right) \tag{1}$$

where ρ is the physical density, N_A is Avogadro's number (6.023×10^{23}), and Z and A are the (effective) atomic number and atomic weight of the traversed material, respectively. Since the ratio Z/A is fairly constant for human tissues, the electron density closely reflects the physical density of the imaged tissue. To avoid the large numbers associated with absolute volume electron density values (which are of the order of 10^{23} electrons/cm^3), it is better to express results in terms of relative volume electron density, which is defined as

$$\eta_e = \frac{\rho_e}{\rho_{e,water}} \tag{2}$$

where $\rho_{e,\text{water}} = 3.343 \times 10^{23}$ electrons/cm^3 is the volume electron density of water.

Ionization and atomic excitation mainly govern the energy loss of protons, and its mean rate (or stopping power) is given by the Bethe-Bloch equation,

$$-\frac{dE}{dx}(\mathbf{r}) = \eta_e(\mathbf{r})\, F(I(\mathbf{r}), E(\mathbf{r})) \tag{3}$$

where $\mathbf{r}$ represents the spatial location, $I(\mathbf{r})$ is the mean ionization potential of the medium, and $E(\mathbf{r})$ is the proton energy, which changes with $\mathbf{r}$ as the proton travels through the medium. Based on the Bethe Bloch equation, the function $F(I(\mathbf{r}), E(\mathbf{r}))$ can be expressed as[1]

$$F(I(\mathbf{r}), E(\mathbf{r})) = K \frac{1}{\beta^2(E)} \left[\ln\left(\frac{2m_e c^2}{I(\mathbf{r})} \frac{\beta^2(E)}{1-\beta^2(E)} \right) - \beta^2(E) \right] \tag{4}$$

where $m_e c^2$ is the electron rest energy, and $\beta(E)$ is the proton velocity relative to c. The constant K is defined as

$$K = 4\pi r_e m_e c^2 \rho_{e,water} = 0.170 \frac{\text{MeV}}{\text{cm}} \tag{5}$$

where r_e is the classical electron radius (2.818×10^{-13} cm). The relationship between β and E is given by

$$\beta(E) = \sqrt{1 - \left(\frac{E_0}{E + E_0} \right)^2} \tag{6}$$

where $E_0 = 938.27$ MeV is the proton rest energy.

Note that the Bethe-Bloch equation (3) is a non-linear first order differential equation of the function $E(\mathbf{r})$. Since $I(\mathbf{r})$ is usually not known in pCT, integration of this equation is not possible. However, for human tissues the variation of I is not very large, and the dependence of the function F on I is relatively weak due to the logarithmic function. Therefore, it is reasonable to assume that $I(\mathbf{r})$ is independent of location and can be replaced by the mean ionization potential of water I_{water} = 61.77 eV. In this case, F is only a function of E and equation (3) can be integrated after separating variables:

$$\int_S \eta_e(\mathbf{r}) dx = \int_{E_{out}}^{E_{in}} \frac{dE}{F(I_{water}, E)} \tag{7}$$

where the integration on the left is along the proton path S, E_{in} is the incident proton energy and E_{out} is the proton energy after traversing the object. It is now obvious that the integrated relative volume electron density can be calculated based on the knowledge of in- and out-going proton energy. Due to the complicated energy dependence of F, the integration must be performed numerically. Also note that the integrated density along the proton trajectory is nothing else than the water-equivalent length of the proton track through the medium. Equation (7) is in the format of the Radon transform if the proton path S is a straight line.

B. Path Estimation

Since protons undergo multiple small deflections by the Coulomb field of the nuclei, the path of each proton deviates from a straight line inside the body and has a zigzag pattern

[1] Note that the formula given here is an approximation of the original Bethe-Bloch equation, which contains a term W_{max}, the maximum energy transfer in a single collision. This approximation is valid if the mass of the incident projectile is large relative to the electron mass, which is the case for protons.

(see Fig. 2(a)). To improve the estimation of the proton path, we used the line L' determined by the entry and exit positions, instead of the proton beam projection line L, provided that the detector can measure both the position and direction of the exiting proton, and the object boundary is roughly known, see Fig. 2(b).

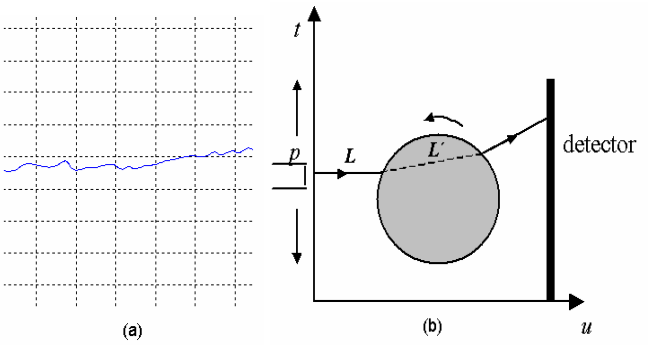

Fig. 2. The "path" of the proton inside the object. (a) The real proton path inside the object is zigzag. (b) Since both the position and direction of the exit proton can be measured and the entry direction is known, the cross-points of the proton beam with the object boundary can be obtained. The proton path, L', is then approximated by the dashed line.

C. *Sinogram Formulation*

While the initial direction of each proton, (*i.e.*, the initial projection ray), is known, the estimated path L', which we call "virtual projection ray", deviates from the original direction, and, therefore, the locations of these virtual rays in sinogram space are usually not uniformly distributed. To apply the conventional FBP reconstruction algorithm, it is necessary to interpolate the virtual projection rays in order to fill a uniform sample space. In this work, a bilinear interpolation method was used according to the pixel-distances in the sinogram.

III. Experimental Results

Simulated pCT scan data were generated by the Geant4 MC simulation code [3]. The phantom was an aluminum disk with 7 rows of holes. The diameter of the disk was 50mm; the diameters of the holes in each row were 4mm, 3mm, 2mm, 1.5mm, 1mm, 0.75mm, and 0.5mm, respectively, see Fig. 3. The average deflection of a 200 MeV proton in such a phantom is comparable to that in human head.

The MC program simulated the transport of 200 MeV mono-energetic protons arriving at the plane u = 0 cm with random heights t, ranging from t = 0 cm to t = 7 cm, and being detected at the plane u = 30 cm. The location and direction of exiting protons were provided by the simulation, as well as their residual energy. Typical profiles of the residual energy versus the initial location for 0^0 and 90^0 are plotted in Fig. 4, and a complete sinogram calculated by interpolations of the virtual projection rays is presented in Fig. 5.

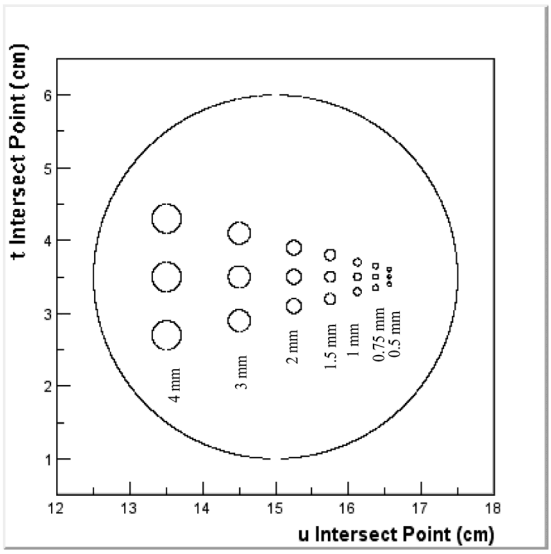

Fig. 3. Lab reference system for the simulations. The phantom is centered at (15, 3.5), the protons arrive along u direction at plane u=0 cm. The detector is at u=30 cm.

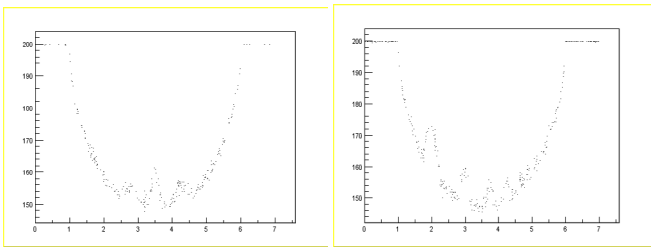

Fig. 4. Residual energy versus entry position at different views: (a) view angle 0^0, (b) view angle 90^0. Some phantom structures are already reflected in these one-view profiles.

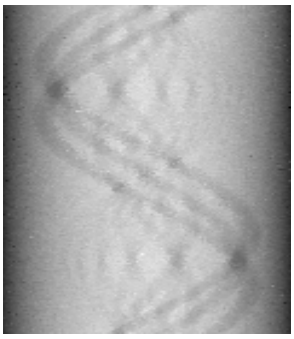

Fig. 5. Sinogram constructed by interpolation of virtual projection rays.

A. *Comparison of Reconstructions using Different Path Estimations*

To study the effect of using different path approximations, a high contrast Al phantom, (Al-disk and air holes), was simulated. A full circular orbit was scanned in 2^o increments, and 350 simulated proton events were generated per projection.

Two images reconstructed with the FBP algorithm are shown in Fig. 6. The left image was obtained using a continuation of the initial proton direction as the inside-path, while the right one used the virtual rays (paths L' in Fig. 2). A relatively large difference between these two results was observed, especially for the boundary and the density contrast. The reconstructed image based on the estimated paths L' is closer to the ground truth.

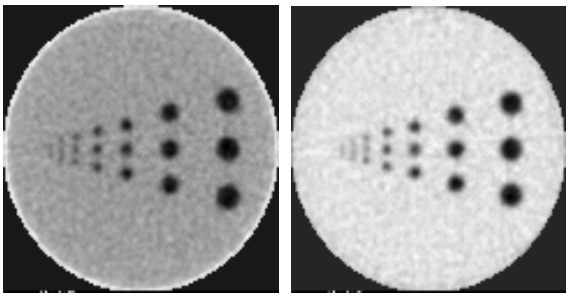

Fig. 6. Reconstructed image using interpolation without (left) and with (right) estimated path L'.

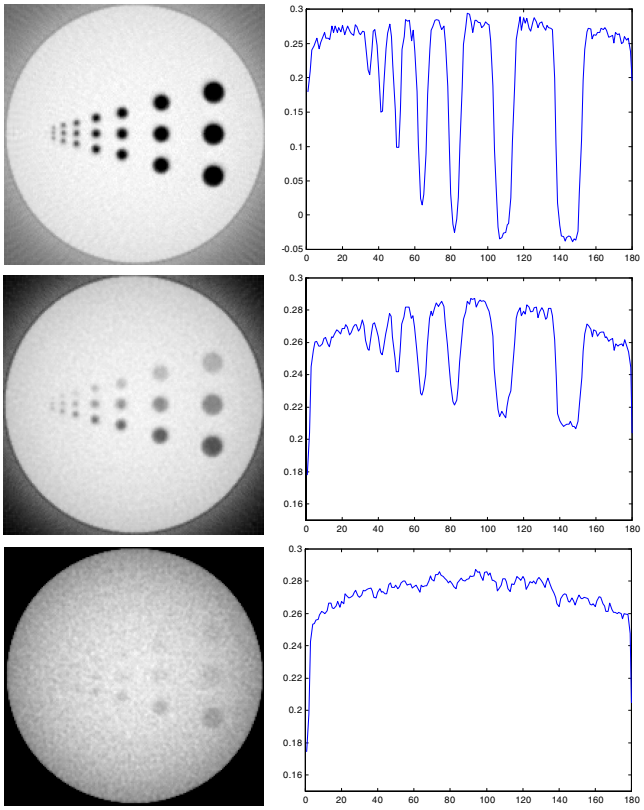

Fig. 7. Reconstructed images and horizontal profiles for different contrast phantom simulations. (Top row: high contrast, middle row: medium contrast; bottom row: low contrast).

B. Contrast Detectability

In this study, the density contrast inside the Al-disk phantom was grouped into three levels: high contrast (Al-disk and air-holes); medium contrast (Al-disk and 90, 80,70% density Al-holes); and low contrast (Al-disk and 99.7, 99, 97% Al-holes). For this study, 35,000 simulated proton events were generated per projection. Reconstructed images using the virtual-ray method are shown in Fig. 7, as well as profiles along the central horizontal line. Note that the display window level for the three images is different. Even at the smallest contrast level, holes are distinguishable down to a diameter of 1.5 mm.

IV. Conclusions

This work demonstrated, in principle, the feasibility of the pCT for clinical use. The GEANT4 MC program can simulate the interaction of charged particles inside materials accurately. Reconstruction using the simple FBP algorithm with a straight-line path estimation can achieve pCT images of relatively high quality, with a high-contrast and high spatial resolution of least 0.5 mm. The path estimation directly impacts the quality of reconstructed image and, therefore, the best possible estimation should be preferred. By the use of the curved "Most Likely Trajectory" (MLT) for pCT image reconstruction is under investigation [4, 5]. With a curved-line proton path, the conventional FBP algorithm is not applicable and has to be modified or re-derived. Sophisticated reconstruction algorithms using maximum likelihood (ML) and/or maximum *a posteriori* probability (MAP) criterion [6, 7, 8] could be another choice for pCT imaging.

V. References

[1] K. Hanson, J. Bradbury, T. Cannon, R. Hutson, D. Laubacher, R. Macek, M. Paciotti and C. Taylor, "Computed tomography using proton energy loss", *Phys. Med. Biology*, **26**: 965-983, 1981.

[2] K. Hanson, J. Bradbury, R. Koeppe, R. Macek, D. Machen, R. Morgado, M. Paciotti, S. Sandford and V. Steward, "Proton computed tomography of human specimens", *Phys. Med. Biology*, **27**: 25-36, 1982.

[3] S. Agostinelli, et al., "GEANT4 - A Simulation Toolkit". *Nucl Instr Meth in Phys Res Section A: Accelerators, Spectrometers, Detectors and Associated Equipment*. **506**(3): 250-303, 2003.

[4] U. Schneider and E. Pedroni, "Multiple Coulomb scattering and spatial resolution in proton radiography," *Med. Physics*, **21**: 1657-1663, 1994.

[5] T. Li, Z. Liang, et al. "Reconstruction with Most Likely Trajectory for Proton Computed Tomography", *SPIE Medical Imaging*, 2004.

[6] L. Shepp and Y. Vardi, "Maximum Likelihood Reconstruction for Emission Tomography", *IEEE Trans. Med. Imaging*, **1**: 113-122, 1982

[7] K. Lange and R. Carson, "EM Reconstruction Algorithms for Emission and Transmission Tomography", *JCAT*, **8**: 306-316 1984.

[8] Z. Liang and H Hart, "Bayesian Reconstruction in Emission Computerized Tomography", *IEEE Trans. Nucl. Sci*, **35**: 877-885, 1988.